

www.acsabm.org Article

# Polymer Surface Dissection for Correlated Microscopic and Compositional Analysis of Bacterial Aggregates during Membrane Biofouling

Mohammadali Masigol,<sup>§</sup> Esther L. Radaha,<sup>§</sup> Arvind D. Kannan, Abigail G. Salberg, Niloufar Fattahi, Prathap Parameswaran, and Ryan R. Hansen\*



Cite This: https://doi.org/10.1021/acsabm.1c00971



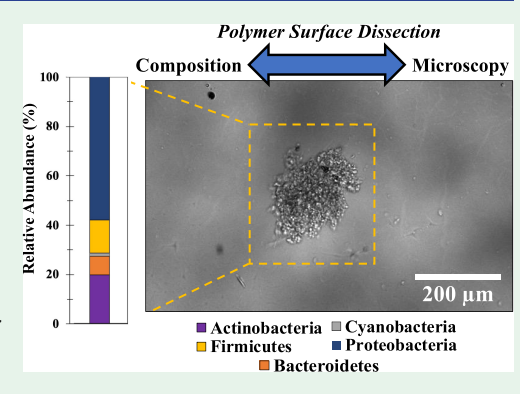
**ACCESS** 

III Metrics & More

Article Recommendations

Supporting Information

ABSTRACT: Multispecies biofilms are a common limitation in membrane bioreactors, causing membrane clogging, degradation, and failure. There is a poor understanding of biological fouling mechanisms in these systems due to the limited number of experimental techniques useful for probing microbial interactions at the membrane interface. Here, we develop a new experimental method, termed polymer surface dissection (PSD), to investigate multispecies assembly processes over membrane surfaces. The PSD method uses photodegradable polyethylene glycol hydrogels functionalized with bioaffinity ligands to bind and detach microscale, microbial aggregates from the membrane for microscopic observation. Subsequent exposure of the hydrogel to high resolution, patterned UV light allows for controlled release of any selected aggregate of desired size at high purity for DNA extraction. Follow-up 16S community analysis reveals aggregate composition, correlating microscopic images with the bacterial



community structure. The optimized approach can isolate aggregates with microscale spatial precision and yields genomic DNA at sufficient quantity and quality for sequencing from aggregates with areas as low as 2000  $\mu$ m<sup>2</sup>, without the need of culturing for sample enrichment. To demonstrate the value of the approach, PSD was used to reveal the composition of microscale aggregates of different sizes during early-stage biofouling of aerobic wastewater communities over PVDF membranes. Larger aggregates exhibited lower diversity of bacterial communities, and a shift in the community structure was found as aggregate size increased to areas between 25,000 and 45,000  $\mu$ m<sup>2</sup>, below which aggregates were more enriched in Bacteroidetes and above which aggregates were more enriched with Proteobacteria. The findings demonstrate that community succession can be observed within microscale aggregates and that the PSD method is useful for identification and characterization of early colonizing bacteria that drive biofouling on membrane surfaces.

KEYWORDS: biofouling, membrane bioreactors, wastewater, hydrogels, cell isolation

# 1. INTRODUCTION

Biofouling refers to the functional or structural disruption of material surfaces due to the assembly of surface-associated microbial communities embedded in a matrix of extracellular polymeric substances (EPS) composed of polysaccharides, proteins, lipids, and nucleic acids. 1,2 Driven by irreversible attachment of early colonizing microbes to a surface followed by EPS expression, growth, and recruitment of additional microbes, biofilms are often compositionally diverse, consisting of unique, interacting microbial species and are spatially heterogeneous at the microscale.<sup>3-7</sup> Despite extensive efforts to mitigate biofilm formation, it often remains an inevitable phenomenon in the food and dairy industry, marine systems, industrial water systems, heat exchange equipment, surgical implants, and medical devices.<sup>8-11</sup> In membrane bioreactor (MBR) wastewater treatment systems specifically, biofouling represents an "Achilles heel", causing deterioration in

membrane permeability and significant decreases in transmembrane pressure, treated water flux, and poor separation efficiency leading to increased energy and operating costs. 12,13

The inability to control fouling in MBR systems is in large part due to a poor understanding of the mechanisms that drive biofilm formation over membrane surfaces, rendering developing foulant layers a black box in MBR operational models. <sup>14</sup> Inspired by well-characterized spatiotemporal models of biofilm assembly, such as biofilm formation in dental plaques, <sup>15</sup> recent research has aimed at providing a better understanding

Received: September 10, 2021 Accepted: November 30, 2021



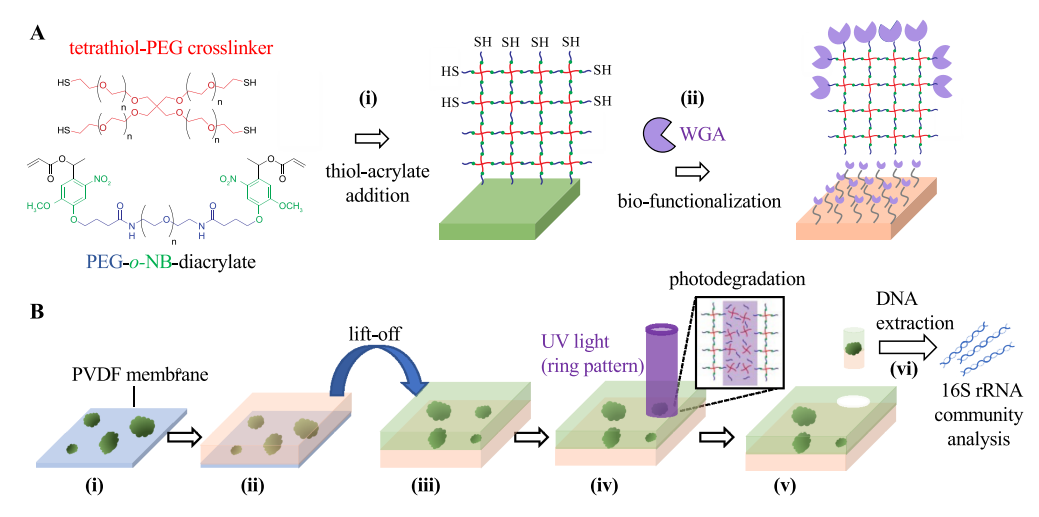


Figure 1. (A) Preparation of biofunctional hydrogels by (i) thiol-acrylate addition of PEG-based macromers and then (ii) functionalization with bioaffinity ligands (WGA). (B) Schematic of the PSD method. (i) A PVDF membrane containing surface-bound microbial biofoulants is (ii) contacted with a ligand-functionalized hydrogel. (iii) The hydrogel is lifted off the membrane surface to detach the aggregates and then covered by a second hydrogel using the same chemistry as in panel (A, i). (iv) Cells of interest are sectioned from the hydrogel base after exposure to UV light patterned in the shape of a ring. (v) Sectioned cells are removed from the hydrogel, and genomic DNA is extracted for 16S rRNA community analysis.

of biofouling mechanisms in MBRs. These efforts have revealed that biofilm formation is not a stochastic process but is mechanistically driven by microbial interactions and, in particular, by early colonizers that first attach to virgin membrane surfaces and then recruit other organisms in progression of the biofilm.<sup>16</sup> Identification of early colonizers may enhance predictive models of membrane biofouling and may inform the development of new antifouling materials and the selection of MBR conditions for improved biofouling control.<sup>17–19</sup> However, little is known about early colonizers as spatially controlled methods for characterizing membrane "hot spots", localized regions of a membrane where early colonizers begin to establish and drive early-stage biofilm development, are lacking.<sup>14</sup>

The gold-standard method of membrane biofilm characterization uses membrane autopsies paired with a combination of molecular and microscopic methods after membrane failure occurs. Because this traditional approach lacks spatial control of cell removal, it provides only a bulk analysis of biofilms present across an entire membrane segment 14,20-22 but not a localized analysis of developing biofilms. Microscopic methods enable one to probe developing biofilms with high spatial resolution and include fluorescence microscopy to study biofilm morphology and porosity, 23-25 atomic force microscopy for measurement of cake-layer surface roughness and of cellular and biomolecular adhesion forces, <sup>24,26,27</sup> and scanning electron microscopy coupled with energy-dispersive X-ray analysis (SEM-EDX). SEM-EDX is valuable because it correlates microscopic information with chemical information, enabling spatial mapping of inorganic chemicals within a biofilm.<sup>28</sup> However, these methods are unable to correlate microscopic information with genomic information because cells cannot be retrieved in a spatially controlled manner after observation. Thus, they are not ideal for biological characterization of membrane hot spots or for identification of early colonizers from wastewater communities. One possibility is to dissect biofilms using laser capture microdissection (LCM), originally developed to harvest cells of interest from tissues for proteomic analysis.<sup>29</sup> However, only a limited number of studies have reported the use of LCM to investigate spatial and compositional heterogeneity in biofilms<sup>30–33</sup> as LCM is destructive to the sectioned cells and the underlying surface.

Photodegradable hydrogels present new capabilities for biofilm characterization. As light can be spatiotemporally controlled, photodegradable hydrogels can be contacted with a heterogeneous collection of cells and then can degrade according to a user-defined light pattern, triggering the selective release of targeted cells from a background of nondesired cells.<sup>34</sup> Using this approach, photodegradable hydrogels have recently been used for retrieval of bacteria from labon-a-chip platforms<sup>35,36</sup> and for use in high-throughput screening and selection of individual bacterial strains from mutant libraries for follow-up genomic analysis. 37,38 Hydrogels consist of poly(ethylene glycol) (PEG) chains modified with photocleavable o-nitrobenzyl (o-NB) chromophores that become cross-linked with a four-arm PEG-thiol through thiol-acrylate Michael-type addition reactions. 39,40 Hydrogel cross-linking chemistry is non-toxic to bacteria and forms 10 nm pores that allow for diffusive exchange of small molecules, making it suitable for culture.<sup>37</sup>

Building off these prior capabilities, here, we develop polymer surface dissection (PSD), a new approach that uses biofunctionalized, photodegradable hydrogels to detach and isolate microbes from membrane surfaces with high spatial precision and high purity without destroying the microbes or the underlying membrane surface. Here, photodegradable hydrogels are first functionalized with affinity ligands (Figure 1A) used to bind and detach microbes from membrane surfaces during a lift-off step. A second hydrogel layer is applied, and microbes are then exposed to high-resolution ring-like patterns of UV light for clean extraction and minimal DNA damage. Sectioned colonies remain encapsulated in hydrogel for additional purification and processing steps, such as DNA extraction for high-throughput community sequencing (Figure 1B)

With the PSD approach, any desired aggregate with an area as low as  $\sim 2000~\mu \text{m}^2$  can be sectioned from a membrane surface to yield genomic DNA of sufficient quantity and quality

for high-throughput 16S community analysis to provide correlated microscopic and compositional analysis of small, developing aggregates. Importantly, the procedure has been optimized to achieve clean extraction and culture-free analysis as culturing for cellular enrichment would inevitably bias the extracted community toward species with higher growth rates. To demonstrate the approach, we use the PSD method to correlate the community structure with aggregate area (5000–  $60,000 \, \mu \text{m}^2$ ) during fouling of aerobic wastewater communities over polyvinylidene difluoride (PVDF) membranes. These findings provide insight into key groups of bacteria from complex wastewater communities that play a role in early stages of biofilm development. Such knowledge is useful for fouling mitigation in MBRs through the rational design of membrane materials tailored against specific microbial groups and by selection of operating conditions that impede the growth of early colonizing microorganisms that have the most influence on the fouling process.

#### 2. MATERIALS AND METHODS

- 2.1. Materials. Triticum vulgare lectin (wheat germ agglutinin, WGA) and poly-L-lysine (PLL) were purchased from Sigma-Aldrich and diluted to specified concentrations in 1× phosphate-buffered saline (PBS) buffer (pH 7.4) and stored at -20 °C. PEG-diacrylate (PEGDA, MW 3400) was purchased from Laysan Bio, and PEG-onitrobenzyl (o-NB) diacrylate was synthesized in-house. The detailed synthesis and H1 NMR characterization of the exact batch of PEG-o-NB-diacrylate used were previously reported and are available from Fattahi et al. 37 Pentaerythritol tetra (mercaptoethyl) polyoxyethylene (4 arm PEG, ((CH<sub>2</sub>)<sub>2</sub>-SH)<sub>4</sub>, MW 10000) was purchased from NOF America Corporation. WGA-Alexa 488 and WGA-Alexa 594 conjugates used for fluorescence microscopy were purchased from Thermo Fisher Scientific, diluted to a 1 mg/mL concentration in 1× PBS (pH 7.4), and stored at -20 °C until use. Escherichia coli JM 109 was stored in 25% glycerol stocks at -80 °C. Ethanol (EtOH), methanol (MeOH), and hydrochloric acid (HCl) were purchased from Thermo Fisher Scientific. Anhydrous toluene (TL), maleimide-PEG-NHS-ester, and (3-mercaptopropyl)trimethoxysilane (MPTS) were purchased from Sigma-Aldrich. A LIVE/DEAD BacLight Bacterial Viability Kit was purchased from Thermo Fisher Scientific and stored at -20 °C until use. FM 1-43 membrane stain was purchased from Thermo Fischer Scientific. PVDF membranes were purchased from Novamem. A QIAamp DNA Micro Kit was purchased from QIAGEN. All chemicals were used as received unless stated otherwise.
- **2.2. Instrumentation.** *2.2.1. Brightfield and Fluorescence Microscopy.* All brightfield and fluorescent images of membranes and hydrogels were taken with an upright microscope (BX51, Olympus) equipped with a 3S camera (Luminara) or an inverted fluorescence microscope (Eclipse Ti-E, Nikon) equipped with a DS-Qi2 monochrome CMOS camera. All images were taken at 10× or 20× magnification, and all fluorescent images were taken with FITC or TRITC filter sets.
- 2.2.2. Polygon400 Light Patterning Instrument. Photodegradable hydrogels were exposed to UV light patterns at micron-scale resolution using a Polygon400 patterned illumination instrument (Mightex Systems) with a 365 nm LED light source (50 W) configured to an Olympus BX51 upright microscope. The area, shape, light intensity  $(0.7-7~\rm mW/mm^2)$ , and irradiation time of each pattern were controlled with Mightex PolyScan2 software. The Polygon400 instrument was calibrated to the specific objective with a mirror and the calibration software prior to each experiment.
- 2.2.3. Attenuated Total Reflection-Fourier Transform Infrared (ATR-FTIR) Spectroscopy. All ATR-FTIR spectra were obtained using a Perkin Elmer Spectrum 400 spectrometer (64 scans) and analyzed using Perkin software to identify an amide peak (~1650 cm<sup>-1</sup>) after functionalization with WGA lectins. The background spectra of a clean, blank ATR crystal were taken prior to measurement, and then,

- the diamond ATR crystal was contacted with WGA-functionalized photodegradable hydrogel surfaces covalently attached to thiolated glass coverslips. The background was subtracted from each spectra, and spectra were baseline-corrected.
- 2.2.4. Measurement of DNA Yield and Quality. DNA yield (260 nm absorbance) and quality (260/280 nm absorbance) of DNA extracted from microbial aggregate samples obtained with the PSD method were measured with a Thermo Scientific Nanodrop One spectrophotometer. DNA quantity measurements were also made with a Qubit 2.0 Fluorometer at the Integrated Genomics Facility at Kansas State University.
- 2.2.5. Plasma Cleaner. A plasma cleaner (model PDC-001-HGP, Harrick Plasma) was used to clean cover slips and glass slides prior to thiolation and perfluoroalkylation using the silane-based reagents.
- 2.2.6. pH Meter. The pH of solutions was determined with an Oakton pH 700 instrument.
- 2.2.7. Image and Statistical Analysis. ImageJ software was used to analyze fluorescent or brightfield images of bacterial cells on surfaces. NIS Elements software was used to quantify lectin fluorescence levels. A MATLAB Statistical Analysis Toolbox and MINITAB 17 software were used to identify statistically significant differences in experimental data. P-values were reported in the text. Information on independent replicates for each experiment is given in the figure captions.
- 2.3. Characterization of Membrane Biofouling. Activated sludge sample solutions obtained from the aeration basin of the Manhattan Wastewater Treatment Plant, KS in 50 mL conical tubes were placed on the bench for 20 min for complete sludge sedimentation to ~15 mL. The supernatant was removed, and the activated sludge was resuspended in 1× PBS solution to ~30 mL followed by vortexing for 10 s. The solution was kept on the bench for another 10 min for complete sludge sedimentation. The supernatant (3 mL) was then harvested. If fluorescence staining was required, then the FM 1-43 membrane stain was then added to the solution at  $4 \mu g$ / mL while shaking at 200 rpm for 30 min at 25 °C to label cells. Cells were washed to remove the unbound dye by centrifugation (2000 rpm, 5 min) and resuspended in  $1 \times PBS$  to an  $OD_{600} = 0.1$ . Novamem membrane filters (PVDF20, 0.02 Micron) of dimensions of  $0.8 \times 0.8 \text{ cm}^2$  were incubated with 3 mL of the processed wastewater solution in a scintillation vial. Scintillation vials were placed in a shaker (200 rpm) for 3–24 h at 25  $^{\circ}$ C. After the desired incubation time, membranes were removed from the solutions and gently washed to remove non-attached cells. Fluorescent images of the membrane surfaces were taken with an inverted fluorescence microscope to determine aggregate size distribution with ImageJ.
- 2.4. Thiol and Perfluoroalkylated Coverslip Fabrication. Functionalization of glass coverslips with thiol groups was used to provide a reactive layer for covalent attachment of hydrogels and was made as previously reported<sup>35</sup> with slight modifications. Briefly, five glass coverslips (1.8 × 1.8 cm) were cleaned with oxygen plasma on each side for 3 min using a Harrick plasma cleaner. Coverslips were then placed vertically and parallel to each other in a glass holder (Wheaton Columbia Jars for Coverslips, part 02-912-636) for subsequent liquid-phase reactions and washing steps. Coverslips were then hydroxylated by contacting with a mixture of 1:1 of MeOH:HCl (37 N) at room temperature (RT) for 1 h, then rinsed in ultrapure water (3  $\times$  20 mL), and dried under N<sub>2</sub>. For functionalization with thiol groups, the coverslips were immersed in MPTS (269 mM) solution in anhydrous TL (5 v/v) at RT for 4 h followed by washing with TL, EtOH/TL (1:1), and EtOH, three times each. The thiol-functionalized coverslips were then dried under N<sub>2</sub> and stored in EtOH at 4 °C until use. The perfluoroalkylated glass slides were prepared as previously reported.3
- **2.5. Hydrogel Substrate Preparation.** Hydrogels were prepared by a Michael-type addition reaction of PEG-o-NB-diacrylate and PEG-tetrathiol. The precursor solution was prepared by adding a 5.6  $\mu$ L solution of PEG-o-NB-diacrylate (49 mM) to 12  $\mu$ L of 1× PBS at pH 8.0. A solution (6.9  $\mu$ L) of PEG-tetrathiol (20 mM) then was added and thoroughly mixed. The precursor solution (7  $\mu$ L) was then quickly pipetted to a perfluoroalkylated glass slide. Two pieces of tape

 $(40.0~\mu m$  thickness each) were placed on the edges of two sides of the thiolated coverslip, and the perfluoroalkylated glass slides with 7  $\mu L$  of precursor solution were placed upside down onto the thiolated coverslip. The thiol-functionalized surface allowed for thiol-acrylate coupling to the surface for stable, covalent hydrogel attachment. The substrate was incubated for 22 min for hydrogel formation. After gelation, the perfluoroalkylated glass slide was gently peeled off to prevent the hydrogel from rupturing, leaving behind the hydrogel attached to the thiolated coverslip.

2.6. Hydrogel Functionalization with Bioaffinity Ligands. WGA was functionalized on hydrogel surfaces to study the effect of affinity molecules for microbe detachment from the membrane surfaces during the PSD procedure (Figure 1A, step ii). For functionalization, hydrogel substrates were first incubated with a 300  $\mu L$  solution of a maleimide-PEG-NHS ester cross-linker in 1× PBS (1.0 mg/mL, pH 6.7) for 2 h followed by washing with the same buffer for 5 min. Hydrogels were then incubated with 300  $\mu$ L solutions of WGA (0.1 mg/mL) in 1× PBS (pH 7.4) for another 2 h and then washed with 1× PBS for 3 min to remove physiosorbed molecules. For characterization of the functionalization step, hydrogels were treated with and without the maleimide-PEG-NHS ester cross-linker, incubated with WGA-Alexa 594 for fluorescence measurements, washed twice with 1× PBS, and once with ultrapure water before soaking in ultrapure water overnight to allow any free molecules to diffuse from the hydrogel. Prior to imaging, hydrogels were allowed to completely dehydrate and then the mean fluorescence intensity of the hydrogel surfaces was measured using a 20× objective and a TRITC filter set with a Nikon inverted fluorescence microscope. For characterization of the functionalization step with ATR-FTIR, all hydrogel surfaces were incubated with maleimide-PEG-NHS ester prior to WGA addition.

2.7. Bacteria Transfer from the Membrane. PVDF membranes were contacted with processed wastewater samples as described in Section 2.3 but without the fluorescent staining step to generate membrane-bound aggregates. Membranes were then placed in contact with biofunctionalized hydrogels (Section 2.6) for 30 min using a 10 g weight to apply uniform pressure and conformal contact between the membrane surface and hydrogel (Figure 1B, step ii). This was followed by detachment of the hydrogel from the membrane. Care was taken in this step to prevent the hydrogel from rupturing. After transfer, hydrogels and membranes were microscopically examined to quantify the size and percent of transferred aggregates. A LIVE/ DEAD BacLight Bacterial Viability Kit was also used to measure bacterial viability after transfer from the membrane to the hydrogels following previous protocols.<sup>41</sup> After transfer, a second hydrogel layer was deposited over the initial hydrogel to trap all non-targeted background cells and provide clean extraction (Figure 1B, step iii). For this, the hydrogel precursor solution (Section 2.5) was pipetted on a perfluoroalkylated glass slide (Section 2.4), then placed upside down on the initial hydrogel, and incubated for 22 min to allow gelation. After formation of the second hydrogel layer, the top glass slide was peeled off gently to prevent the hydrogels from rupturing. Aggregates within the hydrogel were examined using a BX51 upright microscope in brightfield mode to identify target aggregates of specific sizes for extraction.

2.8. Hydrogel Degradation and Aggregate Extraction. Targeted colonies were exposed to patterned UV light using a Polygon400 patterning device configured to an upright BXS1 microscope ( $20\times$  objective,  $2.60~\text{mW/mm}^2$ , 20~s) to section them from the base hydrogel (Figure 1B, steps iv and v). Ring (inner diameter =  $250~\mu\text{m}$ , outer diameter =  $300~\mu\text{m}$ ) and open rectangle ( $112,500~\mu\text{m}^2$  inner rectangle area and  $150,000~\mu\text{m}^2$  outer rectangle area) patterns were used for extraction. Successful extraction of colonies from the hydrogel base was verified by viewing the hydrogel with the BXS1 microscope in brightfield mode during and after exposure. Sectioned parts of the hydrogel containing targeted colonies were extracted into  $200~\mu\text{L}$  of solution (1× PBS, pH 7.4) by suctioning the exposed area with a pipette tip followed by two additional washes, bringing the total liquid volume to  $600~\mu\text{L}$ .

Solutions containing sectioned hydrogel with aggregates were stored at  $-80~^{\circ}\mathrm{C}$  until DNA extraction.

2.9. DNA Extraction. Before proceeding to genomic DNA (gDNA) extraction, most of the liquid volume of each extracted hydrogel-aggregate sample was evaporated using a Thermo Savent DNA120 SpeedVac Concentrator, leaving ~50 μL to maintain the hydrogel-embedded aggregates hydrated. DNA extraction (Figure 1B, step vi) was then performed using a Qiagen QIAamp DNA Micro Kit per the manufacturer's protocol with slight modifications. Briefly, the 50 μL extracted samples were lysed overnight (20 h) at 56 °C with 130  $\mu$ L of buffer ATL and 20  $\mu$ L of Proteinase K solution. A mixture of 1  $\mu$ L of carrierRNA (1  $\mu$ g/ $\mu$ L) in 200  $\mu$ L of buffer AL followed by addition of 200 µL of EtOH to the sample, loaded onto a QIAamp MinElute spin column, washed, and eluted in 50  $\mu$ L of elution buffer. Elution was repeated a second time with a total volume of 100  $\mu$ L to increase DNA yield. Nanodrop 260 and 280 nm absorbance measurements were then used to quantify DNA yield and quality. In addition, Qubit fluorescence measurements were performed since Nanodrop absorbance measurements are known to overestimate DNA concentrations, especially in the presence of carrierRNA.4 Nanodrop absorbance measurement exhibited a 3-fold higher DNA concentration than Qubit fluorescence measurement, confirming this tendency of Nanodrop to overestimate DNA yield (Figure S1A). Therefore, a calibration curve was used to relate Nanodrop measurements to Qubit DNA concentrations (Figure S1B), which are reported in the manuscript. DNA quality measurements were determined by the ratio of absorbance (260/280 nm). All extracted DNA samples were stored at -20 °C before sequencing analysis. Five independent measurements of DNA yield and quality were taken and are reported as average ± standard deviation.

2.10. Community Analysis with 16S rRNA Sequencing. DNA sequencing to determine the bacterial and archaeal composition was performed at MR DNA (Shallowater, TX, USA) on an Illumina Miseq targeting the V4 region of the 16S rRNA gene were used for this purpose. The demultiplexed sequence data files were then imported into QIIME2 software<sup>43</sup> for processing, where the reads were denoised with qiime deblur denoise-16S to obtain error-free representative sequences.<sup>44</sup> After denoising, the resulting high-quality sequence variant data was further used to determine the taxonomic composition in each sample. This was done by assigning taxonomy to the sequences using a pre-trained Naive Bayes classifier trained on the Greengenes 13\_8 99% OTUs for the V4 region (515F/806R) of the 16S rRNA gene. The resulting QIIME2 visual artifact was visualized in the "view.qiime2.org" website as taxonomic bar plots, and the corresponding family/phylum level table was exported to Microsoft Excel as a .CSV file for further processing. The taxonomic table at the family/phylum level was normalized against the total number of bacterial sequences per sample to calculate the relative bacterial abundance (%). Taxonomically unassigned reads were excluded from the relative abundance calculation, and only taxa representing  $\geq 1\%$  of relative abundance in at least one of the samples were used to generate the family level taxonomic heat maps and phylum level bar

# 3. RESULTS AND DISCUSSION

**3.1. Biofunctional Hydrogel Characterization.** The first step in the development of the PSD method was to functionalize hydrogels with affinity ligands to aid in detachment of cells from membrane surfaces during the lift-off step (Figure 1A, steps ii and iii). WGA was chosen as the affinity ligand as it is a lectin that binds with *n*-acetylglucosamine, a glycan commonly present in the extracellular surface components of bacteria, to bind whole bacterial cells at high viability. Prior works demonstrated that WGA-functionalized polymer interfaces could capture bacteria in an efficient and non-destructive manner. Pendent thiol groups present throughout the hydrogel were targeted for WGA functionaliza-

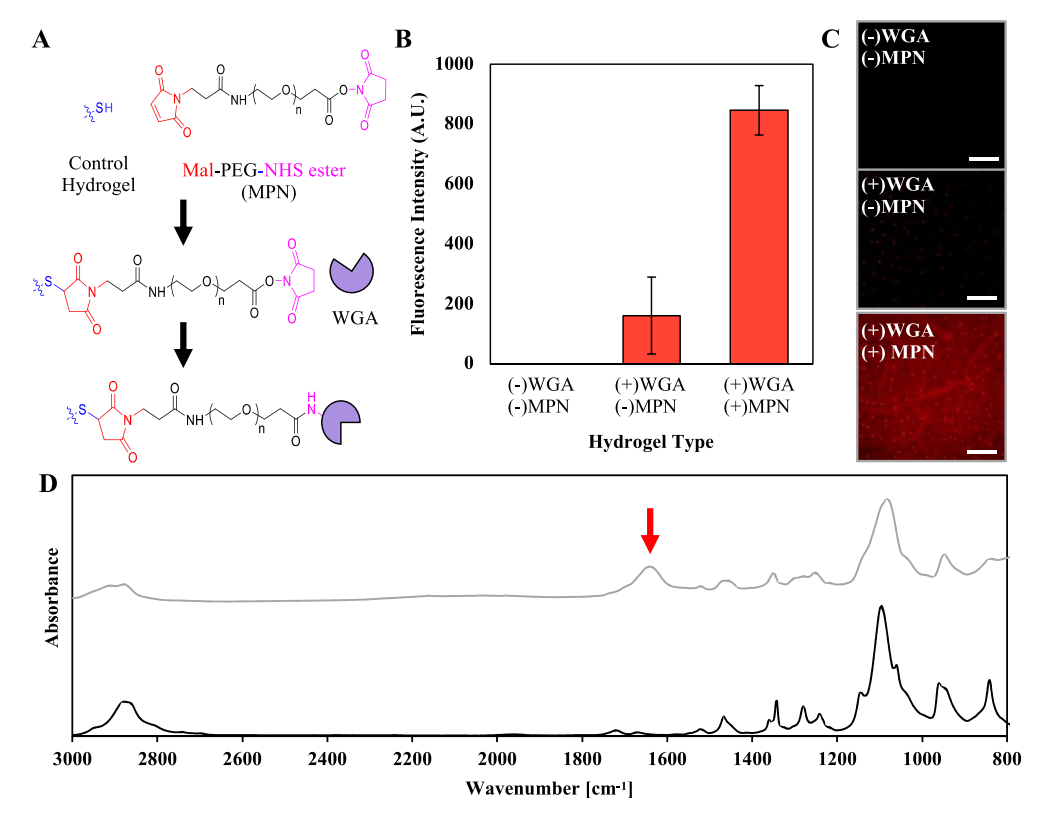


Figure 2. (A) Reaction scheme for functionalization of hydrogels with bioaffinity ligands using Mal-PEG-NHS cross-linkers. (B) Mean fluorescence intensity of background control (non-functional) hydrogels, WGA-A594-functionalized hydrogels without the Mal-PEG-NHS cross-linker, and WGA-A594-functionalized hydrogels pretreated with the Mal-PEG-NHS cross-linker (n=3 independent replicates). (C) Representative fluorescence microscopy images of control hydrogel and hydrogels functionalized with WGA-A594 with and without the Mal-PEG-NHS cross-linker. Scale bars indicate 100  $\mu$ m. (D) FTIR spectra of non-functionalized control hydrogel (bottom) and WGA-functionalized hydrogel (top). The amide functional group is indicated with a red arrow.

tion using a maleimide-PEG-NHS cross-linker, resulting in amine-reactive NHS groups available for secondary coupling with protein affinity ligands (Figure 2A).

To investigate the coupling chemistry on hydrogels formed with the thiol-acrylate Michael addition chemistry, hydrogels were treated with and without the maleimide-PEG-NHS crosslinker, then incubated with WGA-Alexa 594, and characterized with fluorescence microscopy (Figure 2B,C). For background comparison, non-functionalized control hydrogels were also included. Without the cross-linker present, a moderate but significant increase in fluorescence intensity from the control was noted (p < 0.001). This could be due to incomplete conversion of the thiol-acrylate Michael addition throughout the gel, leaving pendent acrylate groups present for biomolecule coupling.<sup>48</sup> When hydrogels were pre-treated with the maleimide-PEG-NHS cross-linker, a significant 5-fold increase in fluorescence intensity was measured (p < 0.001), indicating that the reactivity of the hydrogel toward the affinity ligand was driven by NHS groups present. As secondary verification of biofunctionalization, ATR-FTIR spectra were taken for hydrogels treated with the maleimide-PEG-NHS cross-linker and WGA and compared with the spectra from a non-functionalized control hydrogel. Functionalized hydrogels show an amide (protein) peak at 1650 cm<sup>-1</sup>, indicating the presence of WGA.

After biofunctionalization, the process of bacterial lift-off from a PVDF membrane surface to the hydrogel was investigated as this is a critical step in the PSD method (Figure 1B, steps ii and iii). To verify that the physical contact

between the membrane and hydrogel did not induce damage to either interface during the transfer step, WGA-functionalized hydrogels were contacted with clean PVDF membranes. Qualitative inspection of both surfaces before and after contact showed that no observable damage occurred on either substrate (Figure S2). The transfer of cells from a membrane to the hydrogel and the viability of cells after transfer were also studied. Transfer using non-functionalized PEG hydrogels was also included as a control to elucidate the effect of the WGA affinity ligand on the transfer process. For these initial investigations of the transfer process, *E. coli*, a common member of wastewater communities, was used as a model organism to avoid introducing biological complexities associated with heterogeneous, multispecies wastewater microbial communities.

Different concentrations of *E. coli* (10<sup>6</sup> and 10<sup>7</sup> CFU/mL) were incubated on PVDF membranes for 1.5 h, and functionalized and non-functionalized hydrogels were then placed in contact with the partially fouled membrane for 30 min. After lift-off, image analysis was used to measure the number of bacteria transferred from the PVDF to the hydrogel interface (Figure 3). For both bacterial concentrations, WGA-functionalized hydrogels were capable of detaching *E. coli* cells from the membrane to the hydrogel and showed a significant enhancement compared to the non-functional hydrogel at both concentrations (*P*-value < 0.05). These results confirmed that the addition of affinity ligands to the pre-formed gel matrix enhanced extraction from the membrane during the critical lift-off step in the PSD method. Surprisingly, a significant number

Article

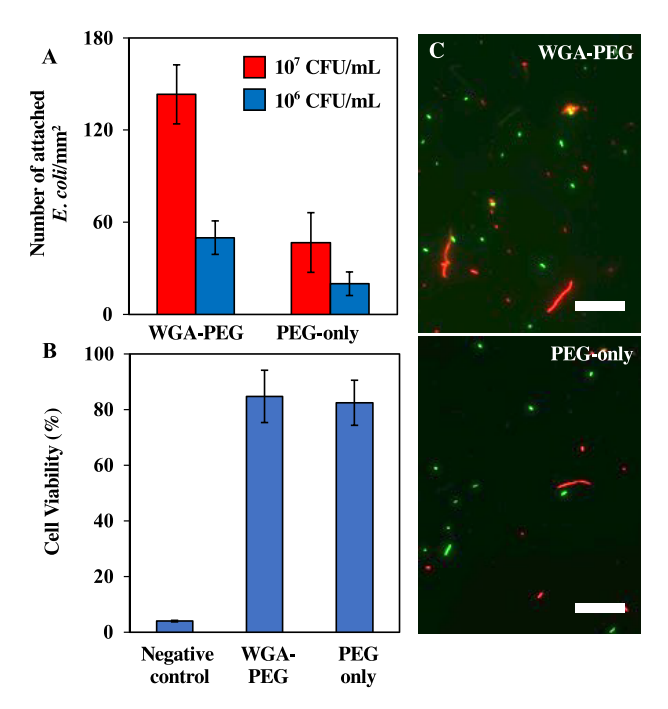


Figure 3. (A) Number of *E. coli* bacterial cells transferred from PVDF membranes to WGA-functional and non-functional hydrogels. (B) Percentage of live cells after contact with WGA-functional and non-functional hydrogels. Negative control: Attached bacteria were exposed to a 2.5% glutaraldehyde solution and 70% isopropanol solution to verify that dead cells could be distinguished with the live/dead assay. (C) Representative fluorescent images from panel (B). All reported values are from n=3 independent replicate hydrogels, and each replicate was imaged at five different surface locations. Images in panel (C) were adjusted to maximize color contrast. Scale bars = 10  $\mu$ m.

of bacteria were also observed to transfer to non-functionalized PEG, despite the fact that PEG is non-adhesive to bacteria. This is possibly due to the presence of pendent, reactive acrylate groups present throughout the hydrogel.

To investigate the viability of cells on the hydrogel interface, 1 mL of E. coli solution (10<sup>6</sup> CFU/mL) was incubated on affinity-functionalized hydrogels for 1 h followed by hydrogel washing with buffer for 3 min. Live/dead staining was then used to evaluate the percentage of live cells attached to the hydrogels. Non-functional hydrogels were again included to decipher the effect of the affinity ligand on cell viability. Cell viability results and corresponding fluorescent images of E. coli on the hydrogel after staining (Figure 3B,C) show that 82  $\pm$ 8.1 and 84  $\pm$  9.4% of attached *E. coli* cells remained alive after contact on non-functionalized hydrogels and WGA-functionalized hydrogels, respectively, indicating that the WGA affinity ligand did not have an effect on cell viability. Because the live/ dead stain deciphers cells based on membrane integrity, this also provides direct evidence that the majority of cells remain intact during the lift-off step.

Removal of live, intact cells was important to avoid premature loss of genomic DNA from cell lysis in downstream processing steps prior to the DNA extraction step (steps iii–v; Figure 1B). Also, isolating live cells enables the option of subsequent culture after the sectioning step (step v; Figure 1) to enrich DNA quantities—if necessary—as bacteria can be cultured within these hydrogels.<sup>37</sup> Finally, live cells enable

further investigation with live cell microscopy to probe specific functionalities within an aggregate, if desired.

**3.2.** Characterization of PVDF Membranes after Wastewater Biofouling. Biofouling from aerobic wastewater communities over PVDF membranes represents a large segment of municipal wastewater treatment systems, where membrane biofouling is responsible for more than 50% of energy expenditures. Given this detrimental impact, this system was chosen for the further development of the PSD approach. The first objective here was to characterize the size distribution of membrane-bound aggregates after contact over the PVDF interface during early-stage (1–24 h) biofouling. Because the PVDF membrane was auto-fluorescent, cells were first treated with a non-specific membrane stain (FM 1-43), providing high contrast for image analysis.

Fluorescence imaging of the fouled membranes revealed aggregates from wastewater samples attached to PVDF membranes (Figure 4A), and increasing aggregate size

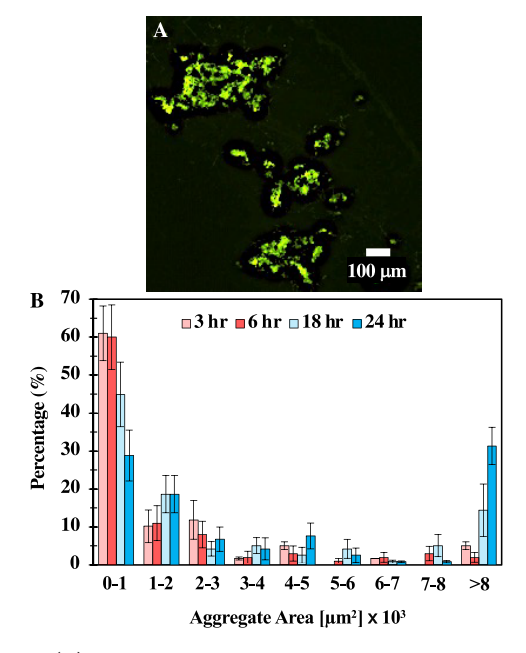


**Figure 4.** (A) Representative fluorescence image of fluorescently labeled wastewater aggregates on a PVDF membrane surface after 24 h of membrane contact time and (B) aggregate size distribution on the PVDF membrane surface after 3, 6, 18, and 24 h contact times. n = 3 independent replicates. Values are the average  $\pm$  standard deviation.

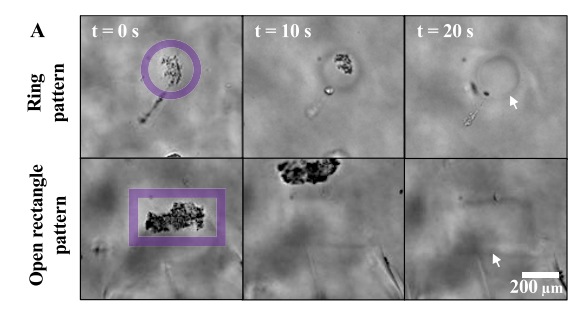
distributions with longer membrane contact times were observed (Figure 4B), consistent with other spatiotemporal investigations of early-stage membrane biofilm formation in membrane bioreactor systems. 19 At early contact times, (3 and 6 h) nearly 60% of all aggregates were small (<1000  $\mu m^2$ ), whereas larger aggregates (>8000  $\mu$ m<sup>2</sup>) represented 5% or less of total aggregates present. The percentage of smaller aggregates (<1000  $\mu$ m<sup>2</sup>) decreased to 45 and 28% for 18 and 24 h contact times, respectively, as larger aggregates developed. When contact time reached 24 h, greater than 20% of aggregates present had areas >8000  $\mu$ m<sup>2</sup>, while smaller aggregates were still present across the membrane. With this observation, contact times >24 h were selected for use in further studies to generate a membrane surface containing a broad distribution of aggregate sizes for further investigation with the PSD approach. After the aggregate size character-

izations, the percentage of membrane-bound aggregates transferred using WGA-functionalized hydrogels with the developed lift-off procedure (Section 3.1) was quantified by imaging membranes before and after lift-off (n = 40 images). On average,  $55 \pm 8.5\%$  of wastewater aggregates were transferred, and a dependence of percent transfer with aggregate size was not observed (Figure S3).

3.3. Aggregate Sectioning and Genomic DNA Extraction. Following the initial characterizations of the hydrogel, of PVDF membrane biofouling, and of the membrane-hydrogel transfer process, the next step was to investigate the sectioning, isolation, and DNA extraction of cells captured within the hydrogel matrix. PVDF membranebound wastewater aggregates were first transferred to WGAfunctionalized hydrogels, and a second hydrogel layer was deposited over the hydrogel-aggregate interface using the same hydrogel precursor solution (Figure 1B, step iii). This ensured that non-targeted aggregates would not be washed off the surface but remain encapsulated in the hydrogel during the sectioning step, enabling specific removal of a targeted aggregate from the hydrogel (Figure 1B, steps iv and v). After deposition of the second layer, hydrogels were inspected with brightfield microscopy. The size of transferred aggregates was first measured, and then, an aggregate of desired area was identified and targeted with patterned UV light (20× objective, 2.60 mW/mm<sup>2</sup>, 20 s) and monitored in real time with brightfield microscopy. Two general light patterns (ring or open rectangle) were used, depending on the size and morphology of the aggregate. Open patterns were used to ensure necessary degradation for release from the hydrogel base while mitigating direct exposure of the targeted aggregates to UV light, which is cytotoxic to bacteria through generation of reactive oxygen species.<sup>51</sup> For larger aggregates (>30,000  $\mu$ m<sup>2</sup>), the ring pattern was found to be insufficient for sectioning, necessitating the use of an open rectangle pattern. Aggregates were observed moving out of the hydrogel after 20 s of exposure, leaving behind all non-targeted regions of the hydrogel and an empty cavity in the hydrogel base from where the aggregate was removed (Figure 5A). Immediately after exposure, media containing the released hydrogel-encapsulated aggregate were suctioned using a pipette for retrieval.

The next goal was to assess the quality and quantity of gDNA extracted from the sectioned hydrogel samples (Figure 1, step vi). As a control to verify that the DNA retrieved from the procedure originated from the targeted colony within the hydrogel, equivalent areas of the hydrogel with no aggregates present were also exposed to UV light and subjected to the DNA extraction protocol under identical conditions. After sectioning, both aggregate-hydrogel samples and blank hydrogel control samples were treated with the Qiagen QIAamp DNA Micro Kit. The sectioned PEG hydrogels had a mesh size of 10 nm,<sup>37</sup> large enough to enable diffusive exchange of biomolecules used in the DNA extraction kit to and from the cell mass (Proteinase K, gDNA) for lysis and DNA extraction. 52 Extraction was followed by evaluation of DNA yield and quality using spectrophotometric absorbance measurements at 260 and 280 nm.

Due to the low number of cells present in a sectioned hydrogel sample, low concentrations of gDNA were expected. Thus, strategies to retain as much DNA as possible were considered, including the use of carrierRNA.<sup>53,54</sup> To investigate this, both the DNA yield and quality after extraction with and without carrierRNA in the DNA extraction



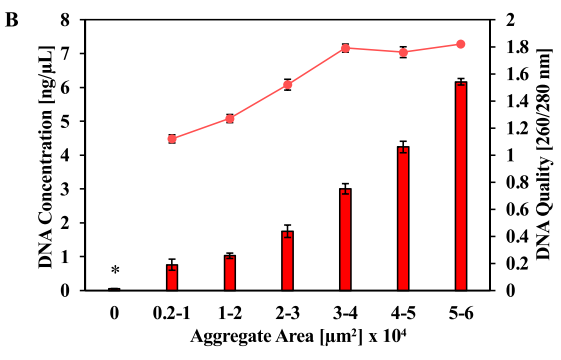


**Figure 5.** (A) Brightfield microscopic images of hydrogels during extraction of targeted aggregates at different time points. Hydrogels containing membrane-extracted wastewater aggregates were exposed a ring pattern or an open rectangle pattern. (B) DNA yield (bar chart) and quality (line plot) at varied wastewater aggregate sizes using the optimized PSD and DNA extraction protocol. Data is adjusted to account for background absorbance from carrierRNA. The asterisk (\*) represents the negative control, which was the quantity of DNA extracted from a blank section of the hydrogel. n = 5 independent replicates.

kit were measured for sectioned hydrogels containing aggregates of varied sizes (Figure S4A,B). In both cases, the trend of increasing DNA yield and DNA quality with increasing aggregate size was observed. However, all aggregates extracted in the absence of carrierRNA resulted in a low DNA yield (<1.3 ng/ $\mu$ L) and low quality (1.0–1.4) (Figure S4A). In the presence of carrierRNA, DNA yield increased by a factor of 4- to 8-fold while DNA quality was also elevated (2.8–3.3) (Figure S4B). However, this was partially due to the presence of carrierRNA that also absorbs at 260 nm. 42 To accommodate this, a control sample containing blank hydrogel and the same amount of carrierRNA was run through the silica column and the resulting absorbance at 260 nm was measured. This was then used to adjust DNA yield and quality. With this correction, the overall DNA yield decreased but showed improvement over samples without carrierRNA, while DNA qualities fell within an acceptable range for genomic analysis. Thus, the use of carrierRNA was found to be critical for achieving sufficient quantities of DNA from sectioned aggregate-hydrogel samples and was used for further DNA extraction in further PSD experiments.

With the fully optimized PSD procedure in place, subsequent investigations of DNA quantity and quality from sectioned hydrogel samples (Figure 5B) determined that aggregates with an area >30,000  $\mu$ m<sup>2</sup> produced ideal DNA qualities (Abs<sub>260</sub>/Ads<sub>280</sub> = 1.8–2.0) and sufficient quantities (>3 ng/ $\mu$ L). As aggregate sizes decreased from 30,000  $\mu$ m<sup>2</sup>, corresponding decreases in both DNA yield and quality were again measured. Aggregates with areas in the range of 2000–10,000  $\mu$ m<sup>2</sup> generated a DNA quantity (0.76 ± 0.16 ng/ $\mu$ L)

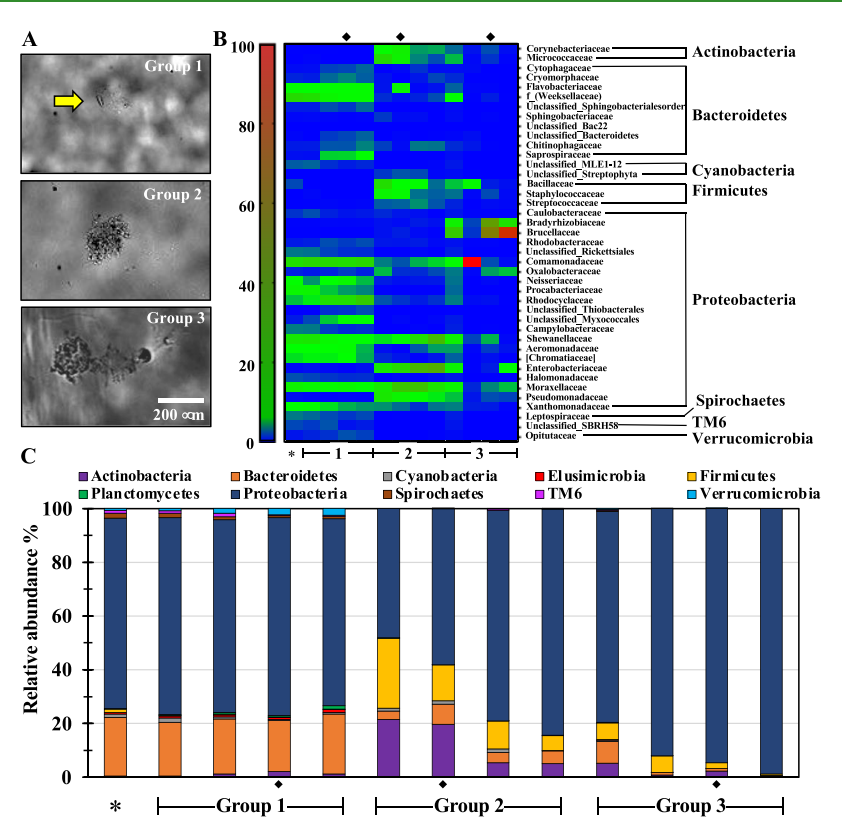


Figure 6. Correlated microscopic and compositional analysis of bacterial aggregates. (A) Brightfield images of an aggregate representative of each group. Groups were binned according to the following area ranges: Group 1:  $5000-25,000 \ \mu\text{m}^2$  (yellow arrow denotes the aggregate), Group 2:  $25,000-45,000 \ \mu\text{m}^2$ , and Group 3:  $45,000-60,000 \ \mu\text{m}^2$ . (B) Heat map distribution of family level bacteria with  $\geq 1\%$  relative abundance at varied aggregate areas, increasing left to right. Phylum groupings are indicated on the far right. (C) Distribution of bacterial phyla with  $\geq 1\%$  relative abundance at varied aggregate areas, increasing left to right. Stars (\*) in panels (B, C) denote the community composition of the wastewater control. Diamonds in panel (B, C) denote the compositions of the aggregates shown in the brightfield images in panel (A).

and quality ( $Abs_{260}/Ads_{280} = 1.12 \pm 0.04$ ) near the lower required limits for genomic analysis but sufficient for PCR amplification and further purification prior to sequencing. Thus, we report this size range as the lowest that can be characterized with the PSD method. Importantly, no significant level of DNA was detected from the blank hydrogel control, ensuring that the isolated DNA originated from aggregates sectioned from the base hydrogel and not from an outside source of contamination.

Finally, it is important to note that these findings do not rely on culturing for sample enrichment. While culturing a solution inoculated with a sectioned sample would likely enable characterization from a significantly lower numbers of initial cells, such an approach would inevitably bias the sample toward microorganisms with favorable metabolism and higher growth rates for a defined nutrient media. As the goal of the PSD method was to provide an accurate depiction of the original aggregate composition during the multispecies assembly processes, culture-based enrichment was successfully avoided.

3.4. Correlated Measurement of the Aggregate Size and Community Structure. After optimization of the DNA extraction procedure, the PSD method was used to investigate the composition of membrane-bound biofilm aggregates at various stages of development by correlating the aggregate size with the community structure. Here, wastewater communities were incubated for 48 h over PVDF membranes to generate membranes containing a large aggregate size distribution, including aggregates large enough (>2000  $\mu$ m<sup>2</sup>) to provide

sufficient DNA yield and quality for 16S community analysis. Following aggregate lift-off, hydrogels were inspected microscopically to identify targeted aggregates ranging in areas between 5000 and 60,000  $\mu \rm m^2$  for sectioning and isolation. Following DNA extraction from each selected aggregate, 16S community analysis was performed to determine the community structure of each individual aggregate, both at the family and phylum level. As a control to verify that all bacteria isolated with the PSD protocol originated from the wastewater sample, 16S community analysis of the wastewater sample was also included.

Correlated microscopic image analysis and 16S community analysis revealed that aggregate composition was dependent on size. Aggregate compositions were first compared to the wastewater control, and all community members found in aggregates were also present in the wastewater control. Aggregates were then binned into three groups based on area: Group 1 (5000–25,000  $\mu$ m<sup>2</sup>, n = 4 samples), Group 2  $(25,000-45,000 \mu m^2, n = 4 \text{ samples}), \text{ and Group 3 } (45,000-45,000 \mu m^2, n = 4 \text{ samples})$ 65,000  $\mu$ m<sup>2</sup>, n = 4 samples) (Figure 6A). Inspection of the relative abundance of aggregates at both the family and phylum level (Figure 6B,C) revealed significant differences in the community structure between aggregates of different size ranges. Most significantly, for small aggregates (Group 1), there was an abundance of Proteobacteria (72  $\pm$  1.8%) and Bacteroidetes (21  $\pm$  1.3%), while Actinobacteria and Firmicutes were minorities (<2%). This community structure was reflective of that from the wastewater control both at the family and phylum level and is consistent with previous studies

on microbial communities in aerobic wastewater treatment systems, where Proteobacteria and Bacteroidetes are found to be the dominant bacterial phyla.  $^{55-57}$  Interestingly, a shift in composition was found in larger aggregates (Group 2), where the composition of Bacteroidetes decreased significantly (p < 0.01), accompanied by an increase in Actinobacteria (13  $\pm$  8.9%) and Firmicutes (14  $\pm$  9.0%). These phyla were diminished in the largest set of aggregates (Group 3), which was dominated by Proteobacteria (91  $\pm$  8.7%). In fact, Proteobacteria became significantly enriched with each aggregate group (p < 0.05), an observation consistent with literature reports demonstrating that the prevalence of Proteobacteria increases as wastewater microbial communities in flocs or biofilms mature.  $^{58-60}$ 

Moreover, Shannon's diversity index was highest for Group 1 aggregates ( $H_1 = 7.3 \pm 0.55$ ), lower for Group 2 aggregates  $(H_2 = 5.3 \pm 0.54)$ , and lowest for Group 3 aggregates  $(H_3 =$  $2.9 \pm 2.27$ ). The drop in diversity and divergence from the overall wastewater composition as aggregates develop in size was driven by the colonization of fewer families of bacteria (Figure 6B). From the Group 3 aggregates analyzed here, specific families of bacteria (Comamonadaceae, Brucellaceae, and Bradyrhizobiaceae) appear enriched, suggesting that specific Proteobacteria from the wastewater community learn to establish themselves as biofilm specialists as aggregates mature in size. Similar conclusions at larger size scales have recently been reported by Lou et al. using membrane autopsies that sample across the entire membrane segment. 19 The new measurement capabilities offered here by the PSD method have enabled observation of microbial succession within membrane aggregates at various stages of development, which, to our knowledge, is the first observation of this phenomena at the microscale.

# 4. CONCLUSIONS

The PSD technique developed here enables isolation of membrane-bound aggregates with microscale resolution and isolation of gDNA suitable for genomic characterization from aggregates with areas as low as  $\sim\!2000~\mu\text{m}^2$  without the need for culture-based enrichment. The key steps in the optimized procedure involve fabrication of photodegradable hydrogels functionalized with bacterial affinity ligands for cell detachment, sealing the extracted cells within the hydrogel, microscopic observation and open-pattern photodegradation for sectioning desired aggregates from the base hydrogel, and efficient gDNA extraction from the sectioned hydrogels using carrierRNA. The approach is novel because it couples genomic information with microscopically observable features of developing microscale biofilms, providing a new genotype-to-phenotype characterization.

The current drawback of the approach is the partial transfer of bacteria between the membrane surface and the hydrogel during the lift-off step. WGA-functionalized hydrogels may select for cells with higher levels of extracellular *n*-acetylglucosamine, and generally, it is possible that the lift-off step could select aggegates more loosely attached to the membrane surface. Transfer with other affinity ligands such as poly-Llysine (PLL) has also been tested with the PSD approach; PLL-functionalized hydrogels were able to transfer bacteria with higher effeciency but lower cell viability than WGA (Figures S5 and S6). However, only complete (100%) membrane-hydrogel transfer efficiency could eliminate all potential bias. This is potentially achieved by applying an

external field to an electrically conductive membrane to force aggregates onto the hydrogel during the transfer step, a strategy similar to capillary electrophoresis for separation of microbial aggregates. 61,62 Even without perfect transfer, the initial demonstration of this approach enabled correlating aggregates of different sizes with the community structure. While these findings (Figure 6) were intended as proof of principle for the PSD approach, the trend of diminished diversity as aggregates mature in size suggests that further investigation will lead to knowledge of specific groups of bacteria within wastewater communities that drive the development of early-stage biofilms. This knowledge is key for predictive models of membrane biofouling and for developing long-term biofouling solutions in MBRs as it may enable one to design anti-fouling membrane materials or find environments and operating conditions that select against these subsets of microorganisms.  $^{16-19}$ 

More broadly, the PSD technique has potential for connecting phenotypic observations of small biofilm aggregates measurable with brightfield or fluorescence microscopy methods with other "omic" or mass spectroscopy-based molecular analysis methods, which may include proteomic, transcriptomic, or EPS compositional analysis of small biofilm aggregates. For example, the PSD method could be used to connect aggregates producing elevated levels of EPS (identified through EPS fluorescence staining) with 16S community analysis and/or transcriptional analysis, a direction currently in pursuit in our laboratory. This could serve to identify subsets of organisms and gene expression pathways leading to EPS production on the membrane, which is a major driver of fouling. These combined efforts will piece together the biological mechanisms that drive biofouling over membranes, knowledge ultimately useful for developing economical and sustainable membrane-based bioseparation processes. Beyond membrane biofouling, the PSD approach also has broader implications for understanding the spatiotemporal development of early biofilms over a variety of other synthetic material interfaces such as urinary catheter surfaces, where multispecies biofilm assembly ultimately leads to catheter-associated urinary tract infections. 63-65

#### ASSOCIATED CONTENT

#### Supporting Information

The Supporting Information is available free of charge at https://pubs.acs.org/doi/10.1021/acsabm.1c00971.

Correlation of DNA quantities using Nanodrop and Qbit measurements, hydrogel and PVDF images before and after lift-off, transfer percent of aggregates from PVDF membranes to WGA-functionalized hydrogels, effect of carrierRNA on DNA yield and quality after extraction from sectioned hydrogels containing varied aggregate sizes, and characterization of transfer and cell viability using PLL-functionalized hydrogels (PDF)

## AUTHOR INFORMATION

## **Corresponding Author**

ı

Ryan R. Hansen — Tim Taylor Department of Chemical Engineering, Kansas State University, Manhattan, Kansas 66506, United States; Occid.org/0000-0002-6471-047X; Phone: +1-785-532-0625; Email: rrhansen@ksu.edu

#### **Authors**

- Mohammadali Masigol Tim Taylor Department of Chemical Engineering, Kansas State University, Manhattan, Kansas 66506, United States; orcid.org/0000-0002-3367-7646
- Esther L. Radaha Tim Taylor Department of Chemical Engineering, Kansas State University, Manhattan, Kansas 66506, United States
- Arvind D. Kannan Department of Civil Engineering, Kansas State University, Manhattan, Kansas 66506, United States
- Abigail G. Salberg Tim Taylor Department of Chemical Engineering, Kansas State University, Manhattan, Kansas 66506, United States
- Niloufar Fattahi Tim Taylor Department of Chemical Engineering, Kansas State University, Manhattan, Kansas 66506, United States
- Prathap Parameswaran Department of Civil Engineering, Kansas State University, Manhattan, Kansas 66506, United States

Complete contact information is available at: https://pubs.acs.org/10.1021/acsabm.1c00971

#### **Author Contributions**

§M.M. and E.L.R. contributed equally as co-first authors. The manuscript was written through contributions of all authors. M.M., E.L.R., P.P., and R.R.H. conceived and designed the experiments. M.M., E.L.R., N.F., and A.G.S. performed the experiments. A.D.K. contributed the analysis tools. M.M., E.L.R., P.P., and R.R.H. wrote the paper. All authors have approved of the final version of this manuscript.

## Notes

The authors declare no competing financial interest.

# ■ ACKNOWLEDGMENTS

This work was supported by the National Science Foundation (award 1805631). A.D.K. and N.F. would like to acknowledge the National Science Foundation Research Trainee Innovations in Food, Energy, and Water Systems (NRT-INFEWS) program (award 1828571). A.G.S. would like to acknowledge the National Science Foundation Research Experiences for Undergraduates (NSF-REU) program (award 1805631).

## REFERENCES

- (1) Donlan, R. M. Biofilms: microbial life on surfaces. *Emerg Infect Dis.* **2002**, *8*, 881–890.
- (2) Costerton, J. Introduction to biofilm. Int. J. Antimicrob. Agents 1999, 11, 217–221.
- (3) Stewart, P. S.; Franklin, M. J. Physiological heterogeneity in biofilms. *Nat. Rev. Microbiol.* **2008**, *6*, 199–210.
- (4) Donlan, R. M.; Costerton, J. W. Biofilms: survival mechanisms of clinically relevant microorganisms. *Clin. Microbiol. Rev.* **2002**, *15*, 167–193.
- (5) Gupta, P.; Sarkar, S.; Das, B.; Bhattacharjee, S.; Tribedi, P. Biofilm, pathogenesis and prevention—a journey to break the wall: a review. *Arch. Microbiol.* **2016**, *198*, 1—15.
- (6) Bjarnsholt, T. The role of bacterial biofilms in chronic infections. *APMIS Suppl.* **2013**, *121*, 1–58.
- (7) Simoes, M.; Simoes, L. C.; Vieira, M. J. A review of current and emergent biofilm control strategies. *LWT-Food Sci. Technol.* **2010**, 43, 573–583.
- (8) Kumar, C. G.; Anand, S. K. Significance of microbial biofilms in food industry: a review. *Int. J. Food Microbiol.* **1998**, *42*, 9–27.

- (9) Angles, M. L.; Chandy, J. P.; Cox, P. T.; Fisher, I. H.; Warnecke, M. R. Implications of biofilm-associated waterborne Cryptosporidium oocysts for the water industry. *Trends Parasitol.* **2007**, *23*, 352–356.
- (10) Khatoon, Z.; McTiernan, C. D.; Suuronen, E. J.; Mah, T. F.; Alarcon, E. I. Bacterial biofilm formation on implantable devices and approaches to its treatment and prevention. *Heliyon* **2018**, *4*, No. e01067.
- (11) Darouiche, R. O. Treatment of infections associated with surgical implants. N. Engl. J. Med. 2004, 350, 1422–1429.
- (12) Flemming, H. C.; Schaule, G.; Griebe, T.; Schmitt, J.; Tamachkiarowa, A. Biofouling the Achilles heel of membrane processes. *Desalination* 1997, 113, 215–225.
- (13) Deng, L.; Guo, W.; Ngo, H. H.; Zhang, H.; Wang, J.; Li, J.; Xia, S.; Wu, Y. Biofouling and control approaches in membrane bioreactors. *Bioresour. Technol.* **2016**, 221, 656–665.
- (14) Meng, F.; Liao, B.; Liang, S.; Yang, F.; Zhang, H.; Song, L. Morphological visualization, componential characterization and microbiological identification of membrane fouling in membrane bioreactors (MBRs). *J. Membr. Sci.* **2010**, *361*, 1–14.
- (15) Kolenbrander, P. E.; Palmer, R. J., Jr.; Periasamy, S.; Jakubovics, N. S. Oral multispecies biofilm development and the key role of cell-cell distance. *Nat. Rev. Microbiol.* **2010**, *8*, 471–480.
- (16) Matar, G. K.; Bagchi, S.; Zhang, K.; Oerther, D. B.; Saikaly, P. E. Membrane biofilm communities in full-scale membrane bioreactors are not randomly assembled and consist of a core microbiome. *Water Res.* **2017**, *123*, 124–133.
- (17) Zhang, K.; Choi, H.; Dionysiou, D. D.; Sorial, G. A.; Oerther, D. B. Identifying pioneer bacterial species responsible for biofouling membrane bioreactors. *Environ. Microbiol.* **2006**, *8*, 433–440.
- (18) Piasecka, A.; Souffreau, C.; Vandepitte, K.; Vanysacker, L.; Bilad, R. M.; Bie, T. D.; Hellemans, B.; Meester, L. D.; Yan, X.; Declerck, P.; Vankelecom, I. F. Analysis of the microbial community structure in a membrane bioreactor during initial stages of filtration. *Biofouling* **2012**, *28*, 225–238.
- (19) Luo, J.; Lv, P.; Zhang, J.; Fane, A. G.; McDougald, D.; Rice, S. A. Succession of biofilm communities responsible for biofouling of membrane bio-reactors (MBRs). *PLoS One* **2017**, *12*, No. e0179855.
- (20) Herrera-Robledo, M.; Morgan-Sagastume, J. M.; Noyola, A. Biofouling and pollutant removal during long-term operation of an anaerobic membrane bioreactor treating municipal wastewater. *Biofouling* **2010**, *26*, 23–30.
- (21) Jun, D.; Kim, Y.; Hafeznezami, S.; Yoo, K.; Hoek, E. M. V.; Kim, J. Biologically induced mineralization in anaerobic membrane bioreactors: Assessment of membrane scaling mechanisms in a long-term pilot study. *J. Membr. Sci.* **2017**, *543*, 342–350.
- (22) Nguyen, T.; Roddick, F. A.; Fan, L. Biofouling of water treatment membranes: a review of the underlying causes, monitoring techniques and control measures. *Membranes* **2012**, *2*, 804–840.
- (23) Yuan, B.; Wang, X.; Tang, C.; Li, X.; Yu, G. In situ observation of the growth of biofouling layer in osmotic membrane bioreactors by multiple fluorescence labeling and confocal laser scanning microscopy. *Water Res.* **2015**, 75, 188–200.
- (24) Lei, Z.; Wang, J.; Leng, L.; Yang, S.; Dzakpasu, M.; Li, Q.; Li, Y.-Y.; Wang, X. C.; Chen, R. New insight into the membrane fouling of anaerobic membrane bioreactors treating sewage: Physicochemical and biological characterization of cake and gel layers. *J. Membr. Sci.* **2021**, *632*, 119383.
- (25) Zhou, Z.; Tan, Y.; Xiao, Y.; Stuckey, D. C. Characterization and Significance of Sub-Visible Particles and Colloids in a Submerged Anaerobic Membrane Bioreactor (SAnMBR). *Environ. Sci. Technol.* **2016**, *50*, 12750–12758.
- (26) Bowen, W. R.; Hilal, N.; Lovitt, R. W.; Wright, C. J. Characterisation of membrane surfaces: direct measurement of biological adhesion using an atomic force microscope. *J. Membr. Sci.* 1999, 154, 205–212.
- (27) Yamamura, H.; Kimura, K.; Okajima, T.; Tokumoto, H.; Watanabe, Y. Affinity of functional groups for membrane surfaces: Implications for physically irreversible fouling. *Environ. Sci. Technol.* **2008**, *42*, 5310–5315.

- (28) Hunter, R. C.; Hitchcock, A. P.; Dynes, J. J.; Obst, M.; Beveridge, T. J. Mapping the speciation of iron in Pseudomonas aeruginosa biofilms using scanning transmission X-ray microscopy. *Environ. Sci. Technol.* **2008**, 42, 8766–8772.
- (29) EmmertBuck, M. R.; Bonner, R. F.; Smith, P. D.; Chuaqui, R. F.; Zhuang, Z. P.; Goldstein, S. R.; Weiss, R. A.; Liotta, L. A. Laser capture microdissection. *Science* **1996**, *274*, 998–1001.
- (30) Perez-Osorio, A. C.; Williamson, K. S.; Franklin, M. J. Heterogeneous rpoS and rhlR mRNA Levels and 16S rRNA/rDNA (rRNA Gene) Ratios within Pseudomonas aeruginosa Biofilms, Sampled by Laser Capture Microdissection. *J. Bacteriol.* **2010**, 192, 2991–3000.
- (31) Podgorny, O. V.; Lazarev, V. N. Laser microdissection: A promising tool for exploring microorganisms and their interactions with hosts. *J. Microbiol. Methods* **2017**, *138*, 82–92.
- (32) Lenz, A. P.; Williamson, K. S.; Pitts, B.; Stewart, P. S.; Franklin, M. J. Localized gene expression in Pseudomonas aeruginosa biofilms. *Appl. Environ. Microbiol.* **2008**, *74*, 4463–4471.
- (33) Perez-Osorio, A. C.; Franklin, M. J. Isolation of RNA and DNA from biofilm samples obtained by laser capture microdissection microscopy. *Cold Spring Harb. Protoc.* **2008**, pdb-prot5065.
- (34) LeValley, P. J.; Tibbitt, M. W.; Noren, B.; Kharkar, P.; Kloxin, A. M.; Anseth, K. S.; Toner, M.; Oakey, J. Immunofunctional photodegradable poly(ethylene glycol) hydrogel surfaces for the capture and release of rare cells. *Colloids Surf.*, B **2019**, 174, 483–492.
- (35) van der Vlies, A. J.; Barua, N.; Nieves-Otero, P. A.; Platt, T. G.; Hansen, R. R. On Demand Release and Retrieval of Bacteria from Microwell Arrays Using Photodegradable Hydrogel Membranes. ACS Appl. Bio Mater. 2019, 2, 266–276.
- (36) Barua, N.; Herken, A. M.; Stern, K. R.; Reese, S.; Powers, R. L.; Morrell-Falvey, J. L.; Platt, T. G.; Hansen, R. R. Simultaneous Discovery of Positive and Negative Interactions Among Rhizosphere Bacteria Using Microwell Recovery Arrays. *Front Microbiol.* **2021**, *11*, 601788.
- (37) Fattahi, N.; Nieves-Otero, P. A.; Masigol, M.; van der Vlies, A. J.; Jensen, R. S.; Hansen, R. R.; Platt, T. G. Photodegradable Hydrogels for Rapid Screening, Isolation, and Genetic Characterization of Bacteria with Rare Phenotypes. *Biomacromolecules* **2020**, *21*, 3140–3151.
- (38) Fattahi, N.; Barua, N.; van der Vlies, A. J.; Hansen, R. R. Photodegradable Hydrogel Interfaces for Bacteria Screening, Selection, and Isolation. *J. Vis. Exp.* **2021**, *177*, No. e63048.
- (39) Tibbitt, M. W.; Kloxin, Â. M.; Sawicki, L.; Anseth, K. S. Mechanical Properties and Degradation of Chain and Step Polymerized Photodegradable Hydrogels. *Macromolecules* **2013**, 46, 2785–2792.
- (40) Kharkar, P. M.; Kiick, K. L.; Kloxin, A. M. Design of Thiol- and Light-sensitive Degradable Hydrogels using Michael-type Addition Reactions. *Polym. Chem.* **2015**, *6*, 5565–5574.
- (41) Masigol, M.; Fattahi, N.; Barua, N.; Lokitz, B. S.; Retterer, S. T.; Platt, T. G.; Hansen, R. R. Identification of Critical Surface Parameters Driving Lectin-Mediated Capture of Bacteria from Solution. *Biomacromolecules* **2019**, *20*, 2852–2863.
- (42) El Bali, L.; Diman, A.; Bernard, A.; Roosens, N. H.; De Keersmaecker, S. C. Comparative study of seven commercial kits for human DNA extraction from urine samples suitable for DNA biomarker-based public health studies. *J. Biomol. Tech.* **2014**, 25, 96–110.
- (43) Bolyen, E.; Rideout, J. R.; Dillon, M. R.; Bokulich, N. A.; Abnet, C. C.; Al-Ghalith, G. A.; Alexander, H.; Alm, E. J.; Arumugam, M.; Asnicar, F.; et al. Reproducible, interactive, scalable and extensible microbiome data science using QIIME 2. *Nat. Biotechnol.* **2019**, *37*, 852–857
- (44) Amir, A.; McDonald, D.; Navas-Molina, J. A.; Kopylova, E.; Morton, J. T.; Xu, Z. Z.; Kightley, E. P.; Thompson, L. R.; Hyde, E. R.; Gonzalez, A.; Knight, R. Deblur Rapidly Resolves Single-Nucleotide Community Sequence Patterns. *MSystems* **2017**, 2, e00191–e00116.

- (45) Hsu, K. L.; Mahal, L. K. A lectin microarray approach for the rapid analysis of bacterial glycans. *Nat. Protoc.* **2006**, *1*, 543–549.
- (46) Hansen, R. R.; Shubert, K. R.; Morrell-Falvey, J. L.; Lokitz, B. S.; Doktycz, M. J.; Retterer, S. T. Microstructured block copolymer surfaces for control of microbe adhesion and aggregation. *Biosensors* **2014**, *4*, 63–75.
- (47) Hansen, R. R.; Hinestrosa, J. P.; Shubert, K. R.; Morrell-Falvey, J. L.; Pelletier, D. A.; Messman, J. M.; Kilbey, S. M.; Lokitz, B. S.; Retterer, S. T. Lectin-Functionalized Poly(glycidyl methacrylate)-block-poly(vinyldimethyl azlactone) Surface Scaffolds for High Avidity Microbial Capture. *Biomacromolecules* **2013**, *14*, 3742–3748.
- (48) Metters, A.; Hubbell, J. Network formation and degradation behavior of hydrogels formed by Michael-type addition reactions. *Biomacromolecules* **2005**, *6*, 290–301.
- (49) Lin, H.; Peng, W.; Zhang, M.; Chen, J.; Hong, H.; Zhang, Y. A review on anaerobic membrane bioreactors: Applications, membrane fouling and future perspectives. *Desalination* **2013**, *314*, 169–188.
- (50) Skouteris, G.; Hermosilla, D.; Lopez, P.; Negro, C.; Blanco, A. Anaerobic membrane bioreactors for wastewater treatment: A review. *Chem. Eng. J.* **2012**, *198*, 138–148.
- (51) Rastogi, R. P.; Richa; Kumar, A.; Tyagi, M. B.; Sinha, R. P. Molecular mechanisms of ultraviolet radiation-induced DNA damage and repair. *J. Nucleic Acids* **2010**, *2010*, 592980.
- (52) Rehmann, M. S.; Skeens, K. M.; Kharkar, P. M.; Ford, E. M.; Maverakis, E.; Lee, K. H.; Kloxin, A. M. Tuning and Predicting Mesh Size and Protein Release from Step Growth Hydrogels. *Biomacromolecules* **2017**, *18*, 3131–3142.
- (53) Kishore, R.; Hardy, W. R.; Anderson, V. J.; Sanchez, N. A.; Buoncristiani, M. R. Optimization of DNA extraction from low-yield and degraded samples using the BioRobot (R) EZ1 and BioRobot (R) M48. *J. Forensic. Sci.* **2006**, *51*, 1055–1061.
- (54) Shaw, K. J.; Thain, L.; Docker, P. T.; Dyer, C. E.; Greenman, J.; Greenway, G. M.; Haswell, S. J. The use of carrier RNA to enhance DNA extraction from microfluidic-based silica monoliths. *Anal. Chim. Acta* **2009**, *652*, 231–233.
- (55) Witzig, R.; Manz, W.; Rosenberger, S.; Kruger, U.; Kraume, M.; Szewzyk, U. Microbiological aspects of a bioreactor with submerged membranes for aerobic treatment of municipal wastewater. *Water Res.* **2002**, *36*, 394–402.
- (56) Nascimento, A. L.; Souza, A. J.; Andrade, P. A. M.; Andreote, F. D.; Coscione, A. R.; Oliveira, F. C.; Regitano, J. B. Sewage Sludge Microbial Structures and Relations to Their Sources, Treatments, and Chemical Attributes. *Front Microbiol.* **2018**, *9*, 1462.
- (57) Qin, H.; Ji, B.; Zhang, S. F.; Kong, Z. H. Study on the bacterial and archaeal community structure and diversity of activated sludge from three wastewater treatment plants. *Mar. Pollut. Bull.* **2018**, *135*, 801–807.
- (58) Griffin, J. S.; Wells, G. F. Regional synchrony in full-scale activated sludge bioreactors due to deterministic microbial community assembly. *ISME J.* **2017**, *11*, 500–511.
- (59) Wilen, B. M.; Onuki, M.; Hermansson, M.; Lumley, D.; Mino, T. Microbial community structure in activated sludge floc analysed by fluorescence in situ hybridization and its relation to floc stability. *Water Res.* **2008**, 42, 2300–2308.
- (60) Wu, L. W.; Ning, D. L.; Zhang, B.; Li, Y.; Zhang, P.; Shan, X. Y.; Zhang, Q. T.; Brown, M.; Li, Z. X.; Van Nostrand, J. D.; et al. Global diversity and biogeography of bacterial communities in wastewater treatment plants. *Nat. Microbiol.* **2019**, *4*, 1183–1195.
- (61) Schneiderheinze, J. M. A. D. W.; Schulte, G.; Westenberg, D. J. High efficiency separation of microbial aggregates using capillary electrophoresis. *FEMS Microbiol. Lett.* **2000**, *189*, 39–44.
- (62) Kartsova, L. A.; Makeeva, D. V.; Kravchenko, A. V.; Moskvichev, D. O.; Polikarpova, D. A. Capillary electrophoresis as a powerful tool for the analyses of bacterial samples. *TrAC, Trends Anal. Chem.* **2021**, *134*, 116110.
- (63) Azevedo, A. S.; Almeida, C.; Melo, L. F.; Azevedo, N. F. Interaction between atypical microorganisms and E. coli in catheter-associated urinary tract biofilms. *Biofouling* **2014**, *30*, 893–902.

(64) Ballen, V.; Ratia, C.; Cepas, V.; Soto, S. M. Enterococcus faecalis inhibits Klebsiella pneumoniae growth in polymicrobial biofilms in a glucose-enriched medium. *Biofouling* **2020**, *36*, 846–861. (65) Cortese, Y. J.; Wagner, V. E.; Tierney, M.; Devine, D.; Fogarty, A. Review of Catheter-Associated Urinary Tract Infections and In Vitro Urinary Tract Models. *J. Healthcare Eng.* **2018**, *2018*, 2986742.

